Adsorption and growth morphology of rare-earth metals on graphene studied by *ab initio* calculations and scanning tunneling microscopy

Xiaojie Liu,[1,2] C. Z. Wang,[2,*] M. Hupalo,[2] Y. X. Yao,[2] M. C. Tringides,[2] W. C. Lu,[1,3,†] and K. M. Ho[2]

[1]*State Key Laboratory of Theoretical and Computational Chemistry, Institute of Theoretical Chemistry, Jilin University, Changchun, Jilin 130021, People's Republic of China*

[2]*Ames Laboratory, U.S. Department of Energy, and Department of Physics and Astronomy, Iowa State University, Ames, Iowa 50011, USA*

[3]*College of Physics, and Laboratory of Fiber Materials and Modern Textile, the Growing Base for State Key Laboratory, Qingdao University, Qingdao, Shandong 266071, People's Republic of China*

(Received 15 August 2010; revised manuscript received 6 November 2010; published 9 December 2010)

Adsorption of rare-earth (RE) adatoms (Nd, Gd, Eu, and Yb) on graphene was studied by first-principles calculations based on the density-functional theory. The calculations show that the hollow site of graphene is the energetically favorable adsorption site for all the RE adatoms studied. The adsorption energies and diffusion barriers of Nd and Gd on graphene are found to be larger than those of Eu and Yb. Comparison with scanning tunneling microscopy experiments for Gd and Eu epitaxially grown on graphene confirms these calculated adsorption and barrier differences, since fractal-like islands are observed for Gd and flat-topped crystalline islands for Eu. The formation of flat Eu islands on graphene can be attributed to its low diffusion barrier and relatively larger ratio of adsorption energy to its bulk cohesive energy. The interactions between the Nd and Gd adatoms and graphene cause noticeable in-plane lattice distortions in the graphene layer. Adsorption of the RE adatoms on graphene also induces significant electric dipole and magnetic moments.

DOI: 10.1103/PhysRevB.82.245408 PACS number(s): 68.43.Bc, 73.22.−f, 68.65.Pq, 73.20.Hb

I. INTRODUCTION

Graphene, a single atomic layer of graphite, has been a material of current intensive studies due to its novel electronic and structural properties and its potential applications in emerging area of carbon-based electronic devices.[1,2] The sp^2 hybridization and unaffected p_z orbitals in graphene are the two prominent characteristics of its electronic structure leading to a unique band structure with a linear dispersion relation near the Dirac point. In addition to the studies of intrinsic behavior of graphene, there has been a lot of interest in modifying the electronic as well as magnetic properties of graphene to meet the needs of various graphene-based materials and device applications. One of the effective ways to control and modify the structure and properties of graphene is by adsorption of atoms and molecules on graphene. Tunable electronic and magnetic properties of graphene are possible through the interactions the graphene with various adsorbed atoms or molecules. Recently, studies of adsorption and diffusion behavior of different adatoms on graphene have also attracted a lot of attentions because the strong in-plane sp^2 hybridization and unaffected p_z orbitals make graphene an interesting substrate for growth of various metal nanostructures for potential applications in nanotechnology.

In the past few years, there has been a rapid growth in first-principles calculations to acquire an electronic and atomic level understanding of the interactions of alkali[3–9] and transition[10–15] metal adatoms on graphene. Many fundamental issues related to these interactions such as stable configurations, adsorption energies and diffusion barriers, dipole moment, and mixed hybridization-induced magnetism between metal adatoms and graphene layer, have been the focus of these studies.[3–15]

It has been shown that most of the alkali and simple metal adsorptions on graphene have low diffusion barriers,[3,9] which are desirable for fast formation of metal islands on the graphene. The ratio of the adsorption energy to the bulk cohesive energy (E_a/E_c) for alkali metal adsorption on graphene is also generally high which would favor the growth of large flat islands on graphene.[3] However, the alkali and simple metals on graphene do not induce significant changes in the electronic and magnetic properties of graphene, although the donation of electrons drive the Fermi level of graphene away from the Dirac point and may induce large dipole moment for the adatom/graphene system.[3] On the other hand, transition metal adsorption on graphene can have significant effects on the structure and electronic properties of graphene[10–15] but the value of E_a/E_c is low. The diffusion barrier of transition metal on graphene is also generally high[3,14] which hinders the formation of big flat metal islands after low-temperature deposition.

While alkali and transition metals adsorption on graphene have been studied extensively, the studies of interactions between rare-earth (RE) metals and graphene are much less. Since the bonding characteristics of RE metals is different from that of *sp* simple metals and transition metals, the study of RE adatom adsorption on graphene would shed additional light into the properties of graphene as well as nanostructure formation mechanism on graphene.

In this paper, using first-principles calculations, we show that adsorptions of RE atoms on graphene exhibit adsorption energies and diffusion barriers intermediate between that of alkali and transition metal adatoms. The adsorption energies and diffusion barriers are also dependent on the choice of RE adatoms. In particular, we found that Eu adsorption on graphene has very low diffusion barrier and at the same time has relatively large adsorption energy with respect to its bulk cohesive energy. Such unique bonding properties of Eu adatom on graphene are desirable for the formation of stable

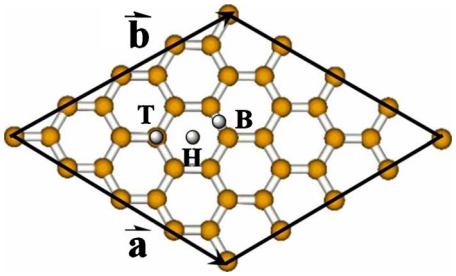

FIG. 1. (Color online) Three adsorption sites for an adatom on graphene: hollow center (H), bridge center (B), and top (T) sites in a periodic 4×4 graphene supercell.

nanostructures on graphene for various fundamental studies as well as technological applications. Scanning tunneling microscopy (STM) experiments of Gd and Eu deposited epitaxially on graphene grown on Si-terminated SiC confirm the differences in the energy barriers and the ratio E_a/E_c by measuring the initial nucleation and subsequent growth morphology. Fractal-like noncrystalline islands are observed for Gd at room temperature (RT) while large crystalline flat-topped islands for Eu. Our calculation also shows that adsorption of RE atoms on graphene layer also enhance the magnetic moments in the system.

II. CALCULATION METHODS

Graphene has a hexagonal primitive unit cell with two carbon atoms per cell. The lattice constant obtained from our calculation is 2.46 Å, agrees well with experimental value. The adatom/graphene system is modeled with one RE adatom in a 4×4 hexagonal graphene supercell with periodic boundary conditions as shown in Fig. 1. The dimension of the supercell in the z direction is 15 Å which allows a vacuum region of about 12 Å to separate the atoms in the supercell and their replicas. The calculations are performed for adatoms positioned on the graphene at the top of a carbon atom, labeled top (T) site, at the middle of a carbon-carbon bond, labeled bridge (B) site, and at the hexagonal center site, labeled hollow (H) site, respectively, as indicated in Fig. 1. Four types RE adatoms, Nd, Gd, Eu, and Yb on graphene have been studied.

The first-principles calculations are performed based on the density-functional theory (DFT) with generalized gradient approximation (GGA) in the form of Perdew-Burke-Ernzerhof[16] implemented in the Vienna *ab initio* simulation package[17–19] (VASP), including spin polarization and dipole moment corrections.[20,21] It is well known that DFT description of the narrow f bands in RE metals based on local-density approximation (LDA) and GGA for exchange-correlation energy functional is not adequate due to the strong electron correlation effects. We adopt the approach in the VASP to cope with this limitation of DFT where the pseudopotentials for RE metals are developed by fixing the f electrons in the core according to the f-electron configuration in the corresponding RE compounds. Yb has a set of completely filled f orbitals which has been naturally treated as core states while the $5p^6$ and $6s^2$ electrons are treated explicitly as valence electrons. For neutral Eu and Gd atoms there are seven f electrons in the ground state. The half-filled f-electron configuration is energetically quite stable and has been put in the core. The $5p^6$ and $6s^2$ electrons of Eu and the $5p^6$, $5d^1$, and $6s^2$ electrons of Gd are treated as valence electrons. Although neutral Nd has four f electrons in the lowest energy configuration, usually one f electron would move out of the core and participate in chemical bonding in bulk environment. Therefore in the VASP, three f electrons are frozen in the core and another f electron and the $5s^2$, $5p^6$, and $6s^2$ electrons are treated as valence electrons. All valence electrons are treated explicitly in the VASP and their interactions with ionic cores are described by projector augmented wave method.[22,23] The wave functions in the present calculation are expanded in a plane wave basis set with an energy cutoff of 600 eV. A k-point sampling of $6\times6\times1$ Monkhorst-Pack grids in the first Brillouin zone of the supercell and a Gaussian smearing with a width of $\sigma=0.05$ eV are used in the calculations. All atoms in the supercell are allowed to relax until the forces on each atom are smaller than 0.01 eV/Å. The supercell dimensions are kept fixed during the relaxation. We have tested the convergences of the energies with respect to the energy cutoff (400 eV vs 600 eV) and k-point sampling ($4\times4\times1$, $5\times5\times1$, and $6\times6\times1$). The results show that the use of 600 eV and a $6\times6\times1$ k-point grid in our calculations should be sufficient.

TABLE I. The adsorption energy (E_a), diffusion barrier (ΔE), electric-dipole moment (P), in-plane graphene lattice distortion amplitude ($d_{//}$), charge transfer (Δq), and magnetic moment (μ_{AG}) for various RE adatoms adsorption on graphene. Magnetic moments of isolated pseudoatoms ($\mu_{A'}$) are also listed for comparison.

Adatom	E_a (eV)	ΔE (eV)	P (D)	$d_{\parallel}$ (Å)	Δq (e)	μ_{AG} (μ_B)	$\mu_{A'}$ (μ_B)
Nd	1.88	0.35	2.61	0.015	0.61	2.30	1.00
Gd	1.61	0.23	1.93	0.016	0.70	2.17	1.00
Eu	0.90	0.14	1.10	0.009	0.62	1.09	0.00
Yb	0.32	0.15	1.17	0.009	1.04	1.09	0.00

III. RESULTS AND DISCUSSIONS

A. Adsorption energy and diffusion barrier

Our calculation results show that the energetically most favorable adsorption site is the H site, followed by the B and then the T sites for all the adatoms studied in this paper. The adsorption energies and diffusion barriers for the four RE metals adsorption on the H site of graphene obtained from our calculations are summarized in Table I. The adsorption energy E_a is defined as the difference between the energy of the relaxed adatom-graphene system and that of the isolated perfect graphene sheet and an isolated RE atom.[3] To minimize the error in the adsorption energy calculations, the energies of the isolated perfect graphene sheet and the isolated atom are also calculated using the same supercell, energy cutoff, and k-point sampling as those in the calculations for the adatom/graphene systems. We have also studied the dif-

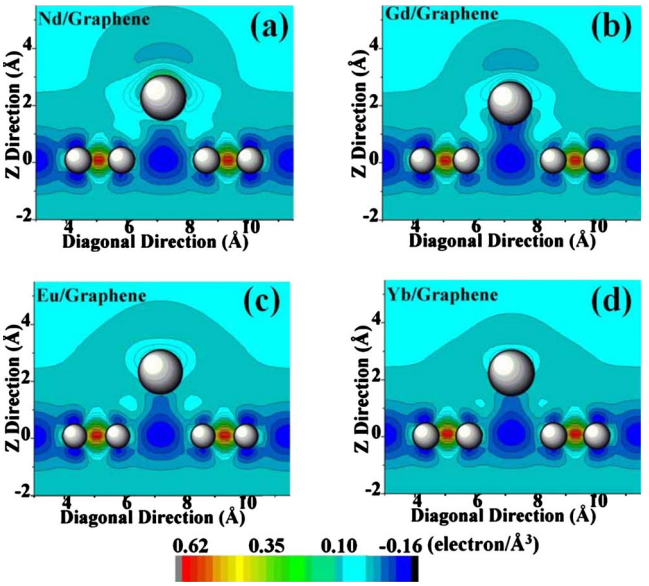

FIG. 2. (Color online) BCD in the vertical diagonal plane of the 4×4 supercell when the RE adatom is located at the H site. Red color means an increase in the electron density and deep blue means a charge density loss, with respect to the superposition of the atomic charge density.

fusion barriers for the adatoms on graphene. Although in principle the diffusion barriers can be obtained by examining the potential-energy surfaces[24,25] for the adatoms on graphene, in the present case the adsorption geometry is relatively simple due to the high symmetry of the graphene lattice. In our present calculation, we determined the adsorption energy and diffusion barrier following the method used in Ref. 3, i.e., the diffusion barrier ΔE is obtained by the energy difference between the H and B sites according to the symmetry.[3] We also further checked the diffusion barrier by examining the potential-energy surface along the line connecting the H site to the B site and then to the next H site similar to the method used in Ref. 10. The diffusion barriers from such calculations are consistent with that determined from the energy difference between the H and B sites. We found that the adsorption energies of Nd and Gd adatoms on graphene are large, 1.88 eV and 1.62 eV, respectively, while that of Eu is intermediate (0.91 eV) and that of Yb is relatively small (0.34 eV). The diffusion barriers are also relatively large for Nd and Gd (0.35 eV and 0.23 eV, respectively) and smaller for Eu (0.14 eV) and Yb (0.15 eV).

The different adsorption energies for different RE adatoms can be explained by their electronic bonding charge distributions (BCD) as shown in Fig. 2. Here the bonding charge distribution is the difference between the self-consistent charge distribution and the simple superposition of atomic charge density of the individual atoms in systems. The bonding charge defined in this way can be regarded as the amount of electrons involved in the bonding. Red color in the plot indicates an increase in the electron density after bonding, and deep blue indicates a charge density loss with respect to the superposition of the atomic charge densities. The region with a higher BCD indicates stronger bond formation in the region. As one can see from Fig. 2, there are noticeable bonding charge distributions between the Nd and Gd adatoms and their nearest carbon atoms from the graphene, suggesting that there is significant covalent bonding between the Nd and Gd adatoms and the graphene which leads to the larger adsorption energies. In comparison, the bonding charge and the degree of covalent bonding between the Eu adatom and graphene is much weaker. There is almost no bonding charge between Yb and graphene layer and the interaction between the Yb adatom and graphene is mainly ionic, similar to the alkali metals on graphene.[3]

B. Experimental study of growth morphology

STM is a useful tool to study metal graphene interaction because the grown island morphology under different conditions, such as different temperature T, coverage θ, and flux rate F, can reveal information about the energetic barriers of metal adsorption and diffusion on graphene. Using STM, we can observe directly whether islands or films are grown at given set of growth conditions and whether they are crystalline or amorphous. STM can also be used to measure the nucleated island density n to deduce the energetic and kinetic parameters to compare with the ones calculated using the first-principles methods. The island density can be analyzed in terms the classical theory of nucleation[26] which has been extensively used in STM experiments to deduce the diffusion barrier ΔE in numerous metal/metal and metal/semiconductor systems.[27] The key assumption of the theory is that as the adatoms are deposited randomly on the surface and diffuse over a distance defined by the diffusion length, they encounter other adatoms and nucleate a stable island if a minimum number of adatoms in the island is reached (the so-called critical size cluster i_c). Very quickly a steady state is attained where all the newly arriving atoms join existing islands and n becomes coverage independent. A high island density n corresponds to slow diffusion while the opposite signifies fast adatom diffusion. Another quantity easily measurable by STM is whether growth is smooth (layer by layer) or rough three dimensional (for the same temperature conditions). The difference in morphology is controlled both by surface diffusion and the step edge barrier, i.e., an extra barrier existing at step edges ΔE_s that controls how easy the atoms move from higher to lower layers. This barrier especially in the first layer is defined by the adatom and the substrate so it also contains information about the strength of the metal-graphene interaction. A small ΔE and ΔE_s imply layer-by-layer growth while in the opposite limit the growth is three dimensional. Both these barriers indirectly reveal information about the strength of the metal-graphene interaction.

STM experiments were carried out for the epitaxial growth of Gd and Eu on graphene prepared by the thermal annealing of SiC. The method produces G1 (single layer) or G2 (bilayer) graphene of very high quality[28] with domains that extend over micromenter because of slow and controlled desorption of Si through the steps to graphitize the surface. The steps undergo a single to triple step transition with different retracting speeds that results in the fine coverage control of the remaining C that eventually produces uniform graphene layers over very long distances.

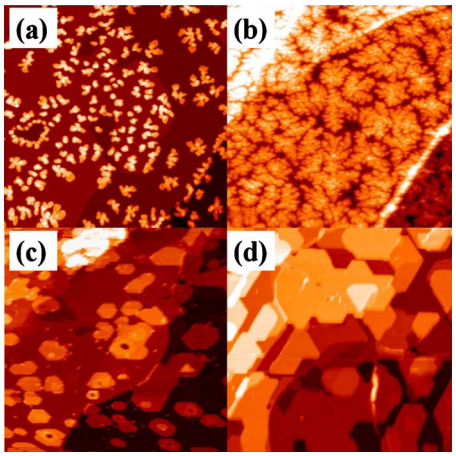

FIG. 3. (Color online) (a) 250×250 nm^2 STM image for $\theta=1$ ML of Gd deposited on graphene at RT with a deposition rate of 0.12 ML/min, which shows fractal-like islands. The islands have preference to nucleate at step edges. The steps are multiples of 0.25 nm the step height of SiC but they are covered with graphene which grows over them. (b) After deposition of $\theta=3.6$ ML of Gd the fractal islands come closer but they do not merge. (c) 250×250 nm^2 STM images for $\theta=1$ ML of Eu deposited on graphene at RT with a deposition rate 0.2 ML/min. The islands are large and crystalline of main height 0.75 nm with well-defined facets. (d) The film closes in a layer-by-layer fashion if the deposition of Eu continues to 3 ML as shown in the STM image of 250×250 nm^2. The barriers are lower and the metal/graphene interaction is weaker for Eu than for Gd as suggested by the calculated barriers in Table I.

Metals were deposited at a rate of 0.12–0.2 ML/min at RT. As seen in Figs. 3(a)–3(d) the grown morphology of Gd [Figs. 3(a) and 3(b)] on graphene at RT is very different from the morphology of Eu [Figs. 3(c) and 3(d)] for similar deposited amounts $\theta\sim1$ and ~3 ML. Gd grows into high density of three-dimentional fractal-like islands. Eu on the other hand shows flat top crystalline islands with well-defined facets. The areas shown in Figs. 3(a)–3(d) are the same 250×250 nm^2. The STM images at the $\theta=1$ ML [Figs. 3(a) and 3(c)] show that the island density is 1.2×10^{-3} islands/nm^2 for Gd vs 4×10^{-4} islands/nm^2 for Eu, and the most common height is five layers for Gd vs three layers for Eu. More importantly the average lateral size is 5 nm for Gd vs 25 nm for Eu. Continuous deposition of Gd results in still fractal islands [see Fig. 3(b)] that spread out laterally and never merge since separate branches of different orientation approach from neighboring islands. On the other hand, continuous deposition of Eu very quickly results in flat films of large terraces seen in Fig. 3(d) with only two or three layers exposed. Gd transforms into hexagonally shaped crystalline islands only when it is heated to a higher temperature 600 °C. These growth morphology differences are consistent with the calculated diffusion barriers listed in Table I. Gd shows relatively higher diffusion barrier and smaller E_a/E_c ratio (0.36) as compared to those of Eu which has a diffusion barrier of 0.14 eV and a E_a/E_c ratio of 0.50. The calculation results can also explain why the high density of fractal islands of Gd on graphene convert to crystalline structure only after heated to higher temperature when the atoms either rearrange or detach and diffuse to other islands. For Eu the diffusion barrier is lower and the E_a/E_c ratio is high which explain why the crystalline islands grow quickly in almost layer-by-layer fashion.

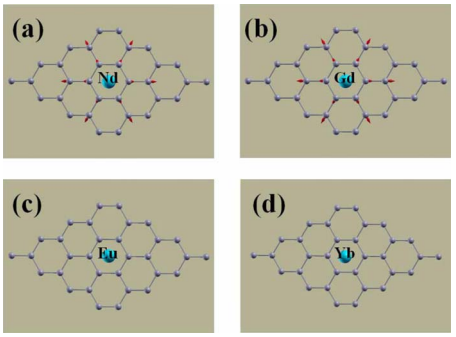

FIG. 4. (Color online) The in-plane lattice distortions of graphene layer due to the adsorption of the RE adatoms. Arrow length represents amplitudes of distortion and arrow direction represents the direction of distortion. The displacements have been enlarged by a factor of 5000 for a clear visualization. Note that there are no visible in-plane distortions for Eu and Yb adsorptions.

C. Dipole moments and lattice distortions

The interactions between RE adatom and graphene induce strong dipole moment in the system. We compute the electric dipole moment p in the z direction for the unit cell of the adatom/graphene system as $p=\int(r-\mathbf{R}_c)\rho_{i+e}(r)d^3r$, where $\mathbf{R}_c$ is the position of net charge distribution, and ρ_{i+e} is charge density of ions and valence electrons. The electric dipole moments from our calculations are summarized in Table I. We can see that a large electric dipole moment especially for Nd/graphene with a value of 2.61 Debye. About 2.0 Debye of electric dipole moment is also found for Gd/graphene. For the more ionic adsorption of Eu and Yb, the total electric dipole moments are about 1.0 Debye. The onset of covalent bonding or ionic bonding between the adatom and graphene also cause different distortions in the graphene layer. In Fig. 4, the in-plane distortions of the graphene layer upon the adsorption of the RE adatoms on the H site of the graphene are plotted. The largest in-plane distortion amplitudes are listed in Table I. These maximum distortions are about 0.6–1.1% of bond length of carbon atoms in the graphene depending on the types of the adatoms. In order to see the distortions more clearly, the displacements indicated by the red arrows in the plots have been enlarged by a factor of 5000 for a better visualization. The distortion patterns (or strain fields) in the graphene layer caused by the adsorption of Nd and Gd are very similar, both have $\sim1.0\%$ in-plane distortion. Note that the in-plane distortion of the second shell carbon atoms with respect to the adatoms is lager than that of the first shell carbon atoms. The lattice distortion in graphene caused by the adsorption of Nd and Gd is not as large as that caused by adsorption of most of the transition metal adatoms. By contrast, there are much smaller in-plane distortion induced by Eu and Yb on graphene. The induced dipole moment and strain field may cause long-range interaction between the adatoms on the graphene and have impor-

TABLE II. Charge transfer among different orbitals in the RE adatom/graphene systems obtained by the Mulliken population analysis based on the QUAMBOs. The unit is in electron. The negative sign means the orbital loses electrons while the positive sign means the orbital gains electrons. The first shell carbon atoms mean the nearest-neighbor carbon atoms of the adatoms.

		Nd	Gd	Eu	Yb
Adatom	$6s$ orbital	−1.31	−1.17	−1.06	−1.04
	$5p$ orbital	0.00	0.00	0.00	0.00
	$5d$ orbital	+0.70	+0.47	+0.45	+0.00
Graphene	p_z orbitals of the first shell carbon atoms	+0.42	+0.54	+0.46	+0.78
	p_z orbitals of the rest carbon atoms	+0.19	+0.16	+0.15	+0.26

tant effects on the growth of the RE metals on the graphene substrate. Further investigations will be needed to understand these effects on the island growth.

D. Charge transfer and induced magnetic moments

Another important feature of adatom/graphene interaction is the charge transfer between adatom and graphene. However, charge transfer is an ambiguous quantity and there is no unique definition. In the literature, charge transfer in adatom-graphene systems has been calculated by integration of charge density in real space or determined from the difference between the density of states (DOS) of the pure graphene and metal adsorbed graphene systems.[3] It was found that the amounts of charge transfer obtained from the two approaches are very different for alkali and simple metals on graphene.[3] While charge transfer may be easier to calculate in the context of ionic bonding, for covalent bonding where charge is shared between adatom and carbon atom of graphene layer, the context of charge transfer is not easy to define in the first-principles calculations using a plane-wave basis set. On the other hand, charge transfer should be better characterized through the popular Mulliken population analysis if the atomic-like local orbitals are used as basis. In this paper, we adopt the recently developed quasiatomic minimal basis orbitals (QUAMBOs) (Refs. 29 and 30) and Mulliken charge analysis method to estimate the amount of charge transfer between the adatom and the graphene layer. The advantage of our QUAMBOs analysis is that it works well for both ionic and covalent bonding systems. In Table I, charge transfer Δq due to the adsorption of the RE adatoms is listed. The positive values of charge transfer indicate transfer of electrons from the adatoms to the graphene. For the RE adatoms studied, there is a noticeable charge transfer from adatoms to graphene layer, especially for Yb where transfer of 1.04 electrons is found. The amount of electron transfer from other three adatoms is about 0.6–0.7 electrons as one can see from Table I.

The Mulliken population analysis based on the QUAMBOs also allows us to gain more detailed information about the charge transfer among the different orbitals. These results are shown in Table II. We can see from Table II that the $6s$ orbital of the RE adatoms gives up more than one electron when the adatoms adsorb on graphene. For Yb on graphene, the 1.04 electrons lost from the $6s$ orbital of the Yb atom all go to the graphene layer. However, for Nd, Gd, and Eu on graphene, about half of the electrons (slightly less for Gd and Eu) given up by the $6s$ orbital of the adatoms occupy the $5d$ orbital of the adatoms thus enhancing the covalent bonding between the adatoms and the graphene. The rest of the electrons are transferred to the graphene layer, mainly to the p_z orbitals of the carbon atoms next to the adatoms. The $5p$ electrons of the adatoms do not participate in the charge transfer and bonding.

We also calculated the magnetic moments of the adatom/graphene systems and compared them to those from the valence electrons of the isolated atoms. Note that the core f electrons of the RE adatoms are not included in the present VASP calculations as discussed in the calculation methods section. Therefore the magnetic moments presented in this paper do not include those from the core f electrons. Since the $4f$ shell of Yb is completely filled, there should be no magnetic moment contribution from the core electrons. For Eu, Gd, and Nd, we found that the f-electron magnetic moment always prefers a parallel alignment with that of outshell s and d electrons in the *ab initio* calculations of isolated atom that include the f electrons explicitly. It is therefore reasonable to assume such parallel alignment hold also for the present case of RE adatom on graphene. From Table I, we can see that the magnetic moments are generally higher when the RE adatoms are adsorbed on graphene. For Nd and Gd, while the magnetic moments from the valance electrons of the isolated atoms are about 1 μ_B, the adatom/graphene system exhibits a magnetic moment of 2 μ_B. Similarly, the adsorptions of Eu and Yb on graphene also induce a magnetic moment of 1 μ_B although there is no magnetic moment from the valence electrons in the isolated Eu and Yb atoms. The enhancement of magnetic moment upon adsorption of RE adatoms on graphene is in contrast to the behaviors of most of the simple and transition metals where the magnetic moments of the adatoms are reduced upon adsorption on graphene.[3,10,11]

To see the origin of the magnetic moment enhancement upon adsorption, we calculated the spin-polarized total electron DOS for the adatom/graphene systems and partial DOS for the adatoms, respectively. The partial DOS from the RE adatoms are also separated into the contributions from the valence electrons with s, p, and d characters, respectively. The DOS are computed using a $12\times12\times1$ Monkhorst-Pack grid for Brillouin-zone sampling and the results are plotted in Fig. 5. From the plot we can see that the magnetic moments

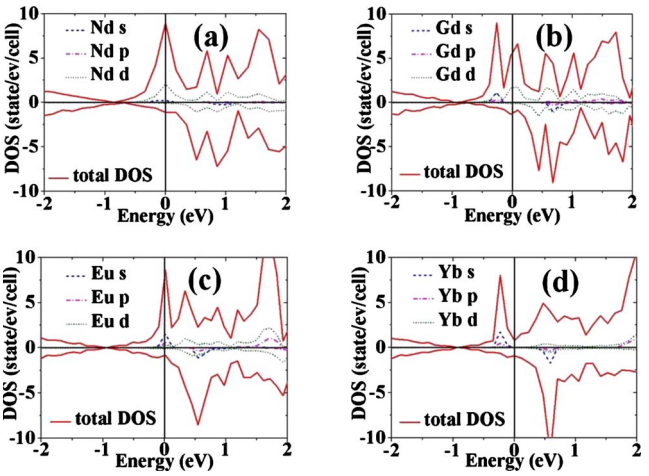

FIG. 5. (Color online) Total density of states of the RE metals adatom-graphene systems (solid line) and the partial density of states of adatoms (dotted lines) for the RE adatoms on the H site.

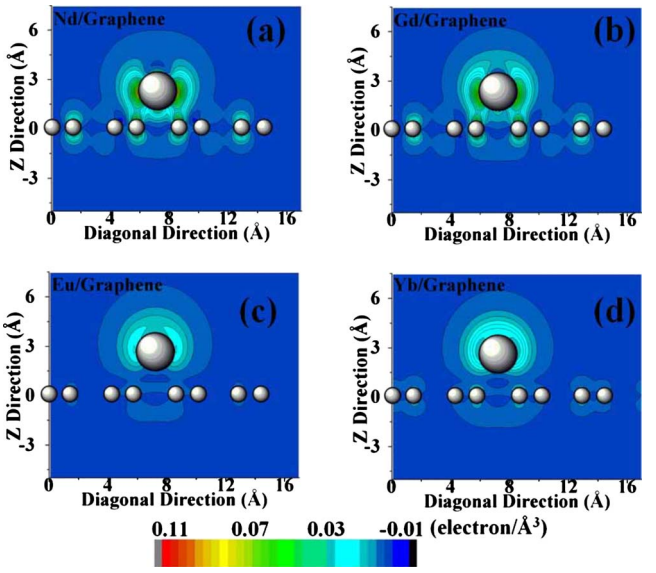

FIG. 6. (Color online) Difference between the spin-up and spin-down charge densities (i.e., magnetization density distribution) in the RE adatom-graphene systems.

in Nd and Eu are from a partially occupied spin-up states right at the Fermi level while for Gd and Yb a spin-up peak between Dirac point and Fermi level is fully occupied. It is interesting to note that the partial DOS from the adatoms exhibit the peaks exactly at the same energies as in the total DOS but the heights of the peaks are much smaller. These features suggest the magnetic moments in the graphene layer are induced by the adsorption of the rare earth atoms. The magnetic moments arise from Nd and Gd exhibit strong *d* electron character while that from Eu and Yb are mainly *s* like. We also plotted the charge density difference between the spin-up and spin-down electrons, as shown in Fig. 6, to see how the magnetization related electrons are distributed in the samples. The results show that there is significant magnetic hybridization between the Nd and Gd adatoms and carbon atoms in the graphene. It is interesting to note that the induced magnetization on the carbon atoms exhibits an alternative shell structure. There are noticeable net spin-up electrons in the odd shells of the carbon atoms from the adatoms but almost zero net charge in the even shells. A similar phenomenon is also observed for the Eu and Yb adatom induced magnetization in the graphene layer but the magnitude is smaller.

IV. SUMMARY

In summary, the adsorption of rare-earth metal adatoms on graphene is studied by first-principles density-functional calculations. The adsorption energies, diffusion barriers, lattice distortions, and electronic and magnetic properties of the RE adatom-graphene systems are studied. While some RE adatoms such as Nd and Gd exhibit covalent bonding with graphene, Eu and Yb display mostly ionic bonding characteristic when adsorbing on graphene. In particular, the adsorption and diffusion behavior of Eu are very special. It has very low diffusion barrier but the adsorption energy is relatively high. The ratio of the adsorption energy to the bulk cohesive energy (E_a/E_c) for Eu adsorption is approximately 0.5 which would favor a layer-by-layer growth of Eu on graphene. In comparison, the E_a/E_c ratio of Gd on graphene is only 0.36 and the diffusion barrier of Gd on graphene is higher than that of Eu, suggesting that the growth morphology of Gd on graphene would be different from that of Eu on graphene. We have also performed STM studies of the growth morphology of Gd and Eu on graphene. The observations from our experiment are consistent with our first-principles calculation results. Gd grows fractal-like islands and crystallizes only when heated to at least 600 °C. Eu grows flat crystalline islands at room temperature and the films continues to grow layer by layer with further metal deposition. It should be noted that the growth morphology of metal islands on graphene is also affected by the step edge barrier ΔE_s which is still difficult to evaluate from first-principles calculations. But from our experimental observation, ΔE_s should be much higher for Gd than Eu, consistent with the other calculated barriers being higher for Gd and suggesting a stronger Gd-graphene interaction. We also note the adsorptions of RE metals on graphene induce strong dipole moments and lattice distortions in the graphene layer (especially for Nd and Gd adsorptions). Since the dipole moment and lattice distortion strain field will introduce long-range interactions, which will also affect the growth morphology of the RE metals on graphene. Further investigations are needed to understand the roles of the long-range dipole and elastic interactions on the growth mechanism of the nanostructures on graphene. Our calculations also show that magnetic moments of the graphene layer are enhanced significantly by the adsorption of the RE adatoms, suggesting that the magnetic properties of graphene can be manipulated through the doping or adsorption.

ACKNOWLEDGMENTS

Work at Ames Laboratory was supported by the U.S. Department of Energy, Basic Energy Sciences, Division of Ma-

terials Science and Engineering including a grant of computer time at the National Energy Research Supercomputing Centre (NERSC) in Berkeley, CA under Contract No. DE-AC02-07CH11358. Xiaojie Liu also acknowledges the support from China Scholarship Council (File No. 2009617104). W.C.L. acknowledges the support by the National Natural Science Foundation of China (Grants No. 20773047 and No. 21043001).

*wangcz@ameslab.gov
†wencailu@jlu.edu.cn

[1] K. S. Novoselov, A. K. Geim, S. V. Morozov, D. Jiang, Y. Zhang, and S. V. Dubonoset, Science **306**, 666 (2004).
[2] A. K. Geim, Science **324**, 1530 (2009).
[3] K. T. Chan, J. B. Neaton, and M. L. Cohen, Phys. Rev. B **77**, 235430 (2008).
[4] Y. Kubota, N. Ozawa, H. Nakanishi, and H. Kasai, J. Phys. Soc. Jpn. **79**, 014601 (2010).
[5] A. Lugo-Solis and I. Vasiliev, Phys. Rev. B **76**, 235431 (2007).
[6] C. Uthaisar, V. Barone, and J. E. Peralta, J. Appl. Phys. **106**, 113715 (2009).
[7] M. Klintenberg, S. Lebègue, M. I. Katsnelson, and O. Eriksson, Phys. Rev. B **81**, 085433 (2010).
[8] K.-H. Jin, S.-M. Choi, and S.-H. Jhi, Phys. Rev. B **82**, 033414 (2010).
[9] T. O. Wehling, M. I. Katsnelson, and A. I. Lichtenstein, Phys. Rev. B **80**, 085428 (2009).
[10] H. Sevinçli, M. Topsakal, E. Durgun, and S. Ciraci, Phys. Rev. B **77**, 195434 (2008).
[11] I. S.-Martinez, A. Felten, J. J. Pireaux, C. Bittencourt, and C. P. Ewels, J. Nanosci. Nanotechnol. **9**, 6171 (2009).
[12] I. Zanella, S. B. Fagan, R. Mota, and A. Fazzio, J. Phys. Chem. C **112**, 9163 (2008).
[13] Q. E. Wang, F. H. Wang, J. X. Shang, and Y. S. Zhou, J. Phys.: Condens. Matter **21**, 485506 (2009).
[14] H. Johll, H. C. Kang, and E. S. Tok, Phys. Rev. B **79**, 245416 (2009).
[15] M. Wu, E.-Z. Liu, M. Y. Ge, and J. Z. Jiang, Appl. Phys. Lett. **94**, 102505 (2009).
[16] J. P. Perdew, K. Burke, and M. Ernzerhof, Phys. Rev. Lett. **77**, 3865 (1996).
[17] G. Kresse and J. Furthmüller, Comput. Mater. Sci. **6**, 15 (1996).
[18] G. Kresse and J. Hafner, Phys. Rev. B **47**, 558 (1993).
[19] G. Kresse and J. Furthmüller, Phys. Rev. B **54**, 11169 (1996).
[20] G. Makov and M. C. Payne, Phys. Rev. B **51**, 4014 (1995).
[21] J. Neugebauer and M. Scheffler, Phys. Rev. B **46**, 16067 (1992).
[22] P. E. Blöchl, Phys. Rev. B **50**, 17953 (1994).
[23] G. Kresse and D. Joubert, Phys. Rev. B **59**, 1758 (1999).
[24] N. Ozawa, N. B. Arboleda, Jr., H. Nakanishi, and H. Kasai, Surf. Sci. **602**, 859 (2008).
[25] N. Ozawa, T. A. Roman, H. Nakanishi, and H. Kasai, J. Appl. Phys. **101**, 123530 (2007).
[26] J. A. Venables, G. D. T. Spiller, and M. Hanbucken, Rep. Prog. Phys. **47**, 399 (1984).
[27] J. W. Evans, P. A. Thiel, and M. C. Bartelt, Surf. Sci. Rep. **61**, 1 (2006).
[28] M. Hupalo, E. H. Conrad, and M. C. Tringides, Phys. Rev. B **80**, 041401(R) (2009).
[29] Y. X. Yao, C. Z. Wang, G. P. Zhang, M. Ji, and K. M. Ho, J. Phys.: Condens. Matter **21**, 235501 (2009).
[30] W. C. Lu, C. Z. Wang, T. L. Chan, K. Ruedenberg, and K. M. Ho, Phys. Rev. B **70**, 041101 (2004).